Characteristic Domain Motion in the Ribosome Recycling Factor Revealed by ^{15}N NMR Relaxation Experiments and Molecular Dynamics Simulations

Takuya Yoshida, Shinichiro Oka, Susumu Uchiyama, Hiroaki Nakano, Tadayuki Kawasaki, Tadayasu Ohkubo, and Yuji Kobayashi*

Graduate School of Pharmaceutical Sciences, Osaka University, 1-6 Yamadaoka, Suita, Osaka 565-0871, Japan

Received November 18, 2002; Revised Manuscript Received February 9, 2003

ABSTRACT: The backbone dynamics of ribosome recycling factor (RRF) from *Escherichia coli* in water were characterized by ^{15}N NMR relaxation analysis and molecular dynamics (MD) simulation. RRF is composed of two domains connected by a joint region that consists of two peptide chains, such that the overall structure seems to mimic that of tRNA. MD trajectories indicated that the relative orientation of domains varies on the nanosecond time scale. We analyzed the observed ^{15}N T_1, T_2, and NOE using an extended model-free spectral density function in which the domain motions with a nanosecond time scale were considered. At 30 °C, the order parameters of slow motion (S_s^2) were determined to be approximately 0.9 for domain I and 0.7 for domain II, respectively. These values indicate that domain I is nearly fixed on the molecular diffusion frame, and domain II is wobbling in a cone for which the semi-angle is about 30°.

After the termination step of protein biosynthesis, the so-called posttermination complex, which is composed of 70S ribosome, deacylated tRNA, and mRNA, remains. In eubacteria, ribosome recycling factor (RRF)[1] is essential for disassembly of the posttermination complex to recycle ribosomes for the next round of protein biosynthesis (for review, see refs *1* and *2*). Three-dimensional structures of RRF from *Thermotoga maritima* (*3*), *Escherichia coli* (*4*, *5*), *Thermus thermophilus* (*6*), *Vibrio parahaemolyticus* (*7*), and *Aquifex aeolicus* (*8*) have been determined by X-ray crystallography and NMR spectroscopy. That work revealed that the structure of RRF is composed of two domains and that one of them, domain I, is a three α helix bundle structure, and the other, domain II, is a three layer $\beta/\alpha/\beta$ sandwich structure. Domain I consists of residues 1−28 and 107−185, and domain II consists of residues 33−101. Because domain I consists of noncontiguous regions in amino acid sequence, the domains are connected by two short peptide segments, residues 29−32 and 102−106.

Except for a crystal structure of detergent-bound RRF from *E. coli* (*4*), the two domains are arranged in a L-shape, such that the overall structures are very similar to that of tRNA in terms of shape and dimensions. It is noteworthy that every structure in the ensemble of solution structures of *A. aeolicus* RRF determined by NMR spectroscopy (*8*) has a characteristic L-shape. In other words, when the bundle axis of domain I is set as the *z* axis, the long axis of domain II exists in the *xy* plane. Interestingly, the rotation angle of domain II around the *z* axis differs in each structure (*7*).

The resemblance of the characteristic L-shape structure of RRF to tRNA structure indicates that RRF binds to the A-site of posttermination complex as a mimic of tRNA. Recently, we found that domain I of RRF is specifically bound to the 50S subunit (*7*). If RRF maintains its tRNA-mimicking structure after the binding, RRF could move to the P-site by EF-G so as to eject deacylated tRNA in a GTP-dependent manner. This postulated behavior of RRF is consistent with the effects of various inhibitors for translocation in the ribosome recycling process (*9*). Specific interactions between RRF and EF-G on ribosome are suggested (*10*, *11*).

Although a detailed mechanism of RRF action is still unclear, a suggestive fact that RRFs from thermophilic bacteria are not comparable to *E. coli* RRF in the assay system containing *E. coli* ribosome and EF-G was shown by several experiments. Atarashi and Kaji suggested that the relative orientation of domains must vary during the reaction and that reduced flexibility of the hinge of RRFs from thermophilic bacteria at the ambient temperature is responsible for the inhibitory effect (*12*). Toyoda et al. examined whether the plasmid encoding mutant *T. thermophilus* RRF is able to rescue the RRF-knockout *E. coli* host. Interestingly, some mutants of *T. thermophilus* RRF, in which the flexibility of the hinge was enhanced, gained an activity in *E. coli* host cells (*6*).

These results indicate that domain motion and/or plasticity for domain arrangement of RRF molecule is important for the activity of RRF. Therefore, to understand the detailed mechanism of RRF action, it is important to establish a way to evaluate the dynamics in a RRF molecule. In fact, no direct evidence about domain motion of RRF in solution has been shown so far. To investigate dynamics of RRF, we performed MD simulation and NMR relaxation analysis in this study.

* To whom correspondence should be addressed. Tel.: +81-6-6879-8220. Fax: +81-6-6879-8224. E-mail: yujik@protein.osaka-u.ac.jp.

[1] Abbreviations: DFM, distance fluctuation map; EF-G, elongation factor G; HSQC, heteronuclear single quantum coherence spectroscopy; MD, molecular dynamics; NMR, nuclear magnetic resonance; NOE, nuclear Overhauser effect; RRF, ribosome recycling factor; T_1, spin−lattice relaxation time; T_2, spin−spin relaxation time; tRNA, transfer RNA.

10.1021/bi027191y CCC: $25.00
Published on Web 03/20/2003

EXPERIMENTAL PROCEDURES

MD Simulations. The MD simulations were performed with GROMACS version 3.1 using GROMACS force field (*13*, *14*). The protein molecule was solvated in a periodic box with the SPC water model (*15*). The clearance between the protein molecule and the edge of the box was at least 9 Å. A particle mesh Ewald method (*16*) was used to calculate electrostatic interactions, with a cutoff of 9 Å for the separation of the direct and reciprocal space summation. van der Waals interactions were truncated at 9 Å. All chemical bonds were constrained using LINCS (*17*), allowing a time step of 2 fs for the integration of the equation of motion. During the MD run, the temperature was controlled using weak coupling (*18*) to a bath of constant temperature. The starting structure of MD for *E. coli* RRF was generated from the crystal structure of the Arg132Gly variant of *E. coli* RRF (*5*) (PDB: 1ISE) by restoring Gly132 to Arg. Since the reported X-ray structure of wild-type *E. coli* RRF (*4*) (PDB: 1EK8) is a complex with a detergent molecule, which affects the structure of domain II and the relative orientation of domains, we used the detergent-free X-ray structure of the Arg132Gly variant of *E. coli* RRF instead. The initial part of simulation consisted of an energy minimization and 21 ps warming steps from 0.1 to 303 K following an equilibration period of 47 ps at 303 K. At the end of this period, the total energy and the temperature were stable. From this point, coordinates were stored every 0.2 ps. The total length of MD run was 4.5 ns.

The essential modes for collective motion (*19*) in a RRF molecule were analyzed using the covariance matrix M of the Cα coordinates x:

$$M_{ij} = \langle (x_i - \langle x_i \rangle)(x_j - \langle x_j \rangle) \rangle \quad (1)$$

The covariance matrix was diagonalized to calculate the eigenvalues and eigenvectors. The principal mode corresponding to the largest eigenvalue describes the representative collective motion. To demonstrate the range and the direction of that motion, the two extreme projections on the average structure were calculated.

The autocorrelation function C(t) for internal motion of the N−H bond vectors was calculated by

$$C(t) = \langle P_2(\mu(0)\mu(t)) \rangle = \sum_{i=1}^{N} P_2(\mu(\tau_i)\mu(t+\tau_i)) \quad (2)$$

where $\mu(t)$ is the N−H unit vector at time t, N is the number of data points used for averaging, and P_2 is the second-rank Legendre polynomial. Coordinate snapshots were superimposed onto the starting structure of MD run by using the backbone atoms to remove the overall motion. The generalized order parameter is defined by a plateau value of the autocorrelation function (*20*, *21*). Although the autocorrelation functions did not converge in the MD run of RRF, a typical autocorrelation function immediately dropped below 1.0 after several picoseconds and then gradually decreased. Thus, we estimated the order parameter for fast motion from

$$S_f^2 = \frac{1}{\Delta T} \int_T^{T+\Delta T} C(t)\, dt \quad (3)$$

where $T = 0$ ps and $\Delta T = 10$ ps.

NMR Experiments. *E. coli* RRF was expressed using pET system (Novagen, Madison, WI) in *E. coli* strain BL21(DE3). Uniformly ^{15}N-labeled protein was obtained by growing cells in M9 medium containing $^{15}NH_4Cl$ as the sole nitrogen source. *E. coli* RRF was purified as described by Kim et al. (*4*). The NMR samples of RRFs were prepared in 90% H_2O/10% D_2O HEPES buffer of 10 mM at pH 7.4 with 50 mM NaCl. A protein concentration of 0.5 mM was used for NMR measurements.

NMR measurements were performed on a Varian INOVA600 spectrometer. Transmitter frequencies for ^{1}H and ^{15}N were 4.76 and 119.0 ppm, respectively. The backbone ^{15}N relaxation parameters T_1, T_2, and ^{15}N-{^{1}H} NOE were measured using HSQC type pulse sequences (*22*−*24*). The T_1 relaxation decay was sampled at six time points (30, 108, 204, 420, 720, and 1050 ms). The T_2 relaxation was measured both by using a ^{15}N spin-locking sequence with a field strength of 2.4 kHz and by using a CPMG-type sequence. The T_2 decay was sampled at six time points (12, 24, 36, 48, 60, and 72 ms). The T_2 values measured using spin-locking were calculated from the decay constant, $T_{1\rho}$, and the T_1 with the resonance offset frequencies and the strength of the spin-lock field. The ^{15}N-{^{1}H} NOE values were derived from two series of spectra, recorded with and without 3.5 s of saturation of the amide protons, respectively. The delay times between scans were about four times the nonselective T_1 value for ^{1}HN. To minimize the effects of spectrometer drift during experiments, all data were measured in an interleaved manner. All experiments were performed twice to check experimental reproducibility. Data were processed using the NmrPipe (*25*), and spectra were analyzed using PIPP (*26*) and in-house written programs. The T_1 and $T_{1\rho}$ values were obtained by nonlinear least-squares fitting of a two-parameter monoexponential function through the peak intensities. Errors in the derived relaxation times were estimated by Monte Carlo type procedures. Resonance assignments were taken from our previously reported results (*27*). Residues undergoing chemical exchange were characterized by variation of values of $T_{2,\mathrm{spinlock}}/T_{2,\mathrm{CPMG}}$ and values of $[(\langle T_2 \rangle - T_2)/\langle T_2 \rangle] - [(\langle T_1 \rangle - T_1)/\langle T_1 \rangle]$ (*28*). In the case of *E. coli* RRF, because both values of each residue were within the range of 1.5 times standard deviation from their mean values in the molecule, chemical exchange contribution to T_2 relaxation was ignored in the following analyses.

Model-Free Analysis. The measured relaxation parameters, T_1, T_2, and ^{15}N-{^{1}H} NOE, are related to the spectral densities by the following equations (*29*):

$$1/T_1 = (d^2/4)[J(\bar{\omega}_H - \bar{\omega}_N) + 3J(\bar{\omega}_N) + 6J(\bar{\omega}_H + \bar{\omega}_N)] + c^2 J(\bar{\omega}_N)$$

$$1/T_2 = (d^2/8)[4J(0) + J(\bar{\omega}_H - \bar{\omega}_N) + 3J(\bar{\omega}_N) + 6J(\bar{\omega}_H) + 6J(\bar{\omega}_H + \bar{\omega}_N)] + (c^2/6)[3J(\bar{\omega}_N) + 4J(0)]$$

$$\mathrm{NOE} = 1 + (d^2/4)(\gamma_H/\gamma_N)[6J(\bar{\omega}_H + \bar{\omega}_N) - J(\bar{\omega}_H - \bar{\omega}_N)]T_1 \quad (4)$$

where $d = [\mu_0 h \gamma_N \gamma_H/(8\pi^2)]\langle 1/r^3_{NH} \rangle$, $c^2 = (\omega_N^2/3)(\Delta\sigma)^2$, ω_N and ω_H are the Lamor frequencies of the ^{15}N and ^{1}H nuclei,

respectively, μ_0 is the permeability of free space, γ_N and γ_H are the gyromagnetic ratios of ^{15}N and ^{1}H, h is Planck's constant, r_{NH} is the length of the amide bond, and $\Delta\sigma$ is ^{15}N CSA value, which is the difference between parallel and perpendicular components of the ^{15}N chemical shift tensor. The value of -172 ppm was used as ^{15}N CSA (*30*).

Because the RRF molecule has a very anisotropic shape, spectral densities should depend on the orientation of the N−H internuclear vectors and on their fluctuations relative to the diffusion tensor. In the case of an axially symmetric diffusion tensor ($\mathbf{D}_{xx} = \mathbf{D}_{yy}$), the model-free spectral density function (*20*, *21*) at a frequency ω is approximated by

$$J(\bar{\omega}) = \frac{2}{5}\sum_{j=1}^{3} A_j \left[\frac{S^2\tau_j}{1+(\bar{\omega}\tau_j)^2} + \frac{(1-S^2)\tau_j^e}{1+(\bar{\omega}\tau_j^e)^2}\right] \quad (5)$$

with

$$A_1 = 0.75\sin^4\alpha, A_2 = 3\sin^2\alpha\cos^2\alpha, A_3 = (1.5\cos^2\alpha - 0.5)^2$$

$$\tau_1 = (4\mathbf{D}_{zz} + 2\mathbf{D}_{xx})^{-1}, \tau_2 = (\mathbf{D}_{zz} + 5\mathbf{D}_{xx})^{-1}, \tau_3 = (6\mathbf{D}_{xx})^{-1}$$

where α is the angle between the principal axis of the axially symmetrical diffusion tensor and the N−H vector.

To test the validity of simple model-free analysis on the internal motion and the rotational diffusion property of RRF, experimental relaxation data for residues were fitted with the model function (*5*) by using the program Model-Free (*31*). In this analysis, the data for residues in well-defined secondary structure were used for fitting with an axially symmetrical diffusion tensor. Relative orientations of N−H bond vectors were obtained from the crystal structure. To take into account the possibility that the relative orientation of domains in the crystal differ from that in solution, each domain was rotated to align its principal axis of the diffusion tensor to the z axis before the calculation for the whole molecule.

Extended Model-Free Analysis for Domain Motion. To evaluate the rigid body motion for each domain, observed relaxation data were fitted with the model function

$$J(\bar{\omega}) = \frac{2}{5}\sum_{j=1}^{5} A_j \left[\frac{S_f^2 S_s^2\tau_j}{1+(\bar{\omega}\tau_j)^2} + \frac{S_f^2(1-S_s^2)\tau_j^s}{1+(\bar{\omega}\tau_j^s)^2} + \frac{(1-S_f^2)\tau_j^f}{1+(\bar{\omega}\tau_j^s)^2}\right] \quad (6)$$

with

$$1/\tau_j^i = 1/\tau_j + 1/\tau_i \text{ where } i = \text{s or f}.$$

This function has the same form as the extended model-free spectral density function in which the slow and fast motions have different correlation times (τ_s, τ_f) and order parameters (S_f, S_s). Clore et al. introduced this function for analyzing local slow motion in flexible region of a protein (*32*). In the present analysis, we applied the function for analyzing the collective motion of each domain. For this purpose, τ_s was forced to be uniform for each domain. To take account of anisotropy of domain motion, the order parameter for the motion on a slow time scale, S_s, was optimized for each residue. The order parameter for fast local motion, S_f, was fixed at the value obtained from the MD trajectory. The correlation time for fast local motion, τ_f, was approximated to be zero. In this model, we assume that each domain moves in a molecular frame that tumbles in solution and that the domain motion is decoupled from the rotational diffusion of the molecule. Therefore, the rotational diffusion tensor was optimized globally for a molecule. ^{15}N T_1, T_2, and ^{15}N-{^{1}H} NOE data were fitted simultaneously on the basis of the atomic coordinates optimizing parameters described above. In this procedure, the average orientation of the long axis of the rotational diffusion tensor relative to the coordinates of each domain was also optimized. In consideration of the results of MD, where each domain of RRF molecule diffuses within a limited range, that value was restricted within the range sampled in MD trajectory. We found, however, that the relative orientation of each domain has little effect on calculated order parameters (data not shown). All calculations were done with an in-house written program. Similar applications of the extended model-free spectral density function were recently reported (*33*, *34*).

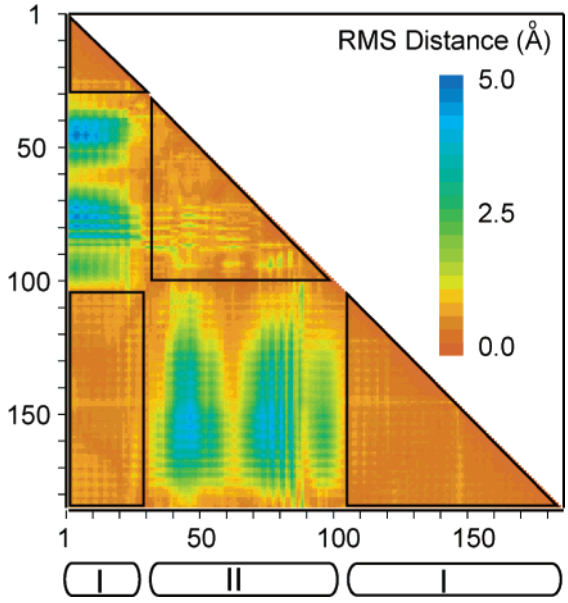

FIGURE 1: Distance fluctuation maps (DFM) calculated from 4.5 ns MD trajectories for *E. coli* RRF. DFM represents the fluctuation of distances between two Ca atoms, R_{ij}.

RESULTS

MD Simulations. To analyze the domain structure of the RRF molecule, a distance fluctuation map (DFM) (*35*) was calculated. The DFM revealed characteristic domain structure of the RRF molecule as shown in Figure 1. The triangles and rectangle in DFM demonstrate that the distance fluctuations inside each domain are smaller than those between domains. In other words, we have confirmed the composition of domain structure from a dynamic point of view. Essential dynamics analysis using the covariance matrix revealed domain motion. As shown in Figure 2A, a dominant collective motion corresponding to the largest eigenvalue exists in the RRF molecule. This motion is a variation of the relative arrangement of domains (Figure 2B,C). Characteristic dynamics were also found in rms deviations (RMSD) of Cα coordinates during simulation from mean

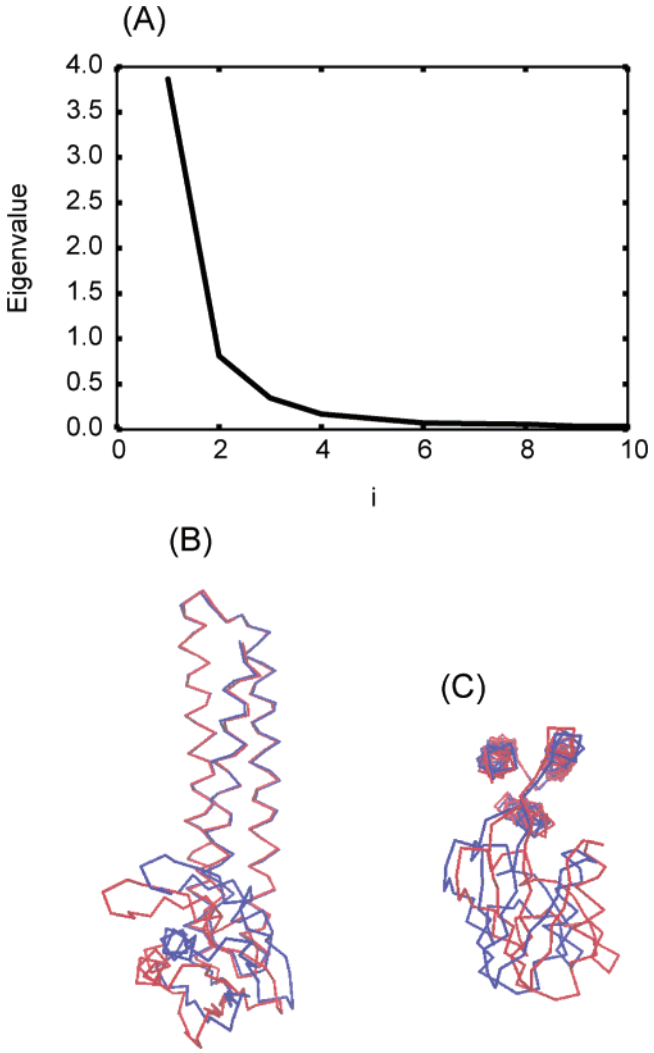

FIGURE 2: Essential dynamics analysis for 4.5 ns MD trajectories of *E. coli* RRF. (A) First 10 eigenvalues. (B and C) The two extreme projections for the motion corresponding to the largest eigenvalue are superimposed for the best fit over domain I.

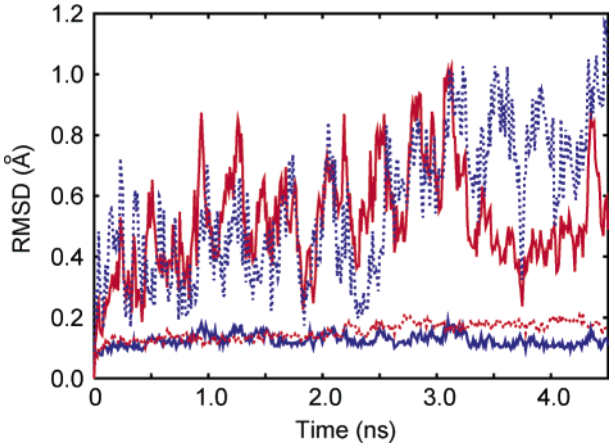

FIGURE 3: Time evolution of Cα root-mean-square deviations (RMSDs) with respect to the initial structure. RMSD of domain I superimposed for the best fit over itself (solid blue line), RMSD of domain I superimposed for the best fit over domain II (dashed blue line), RMSD of domain II superimposed for the best fit over domain I (solid red line), and RMSD of domain II superimposed for the best fit over itself (dashed red line).

structure as shown in Figure 3. When only domain I is used for superposition in calculation of RMSD, the RMSD value

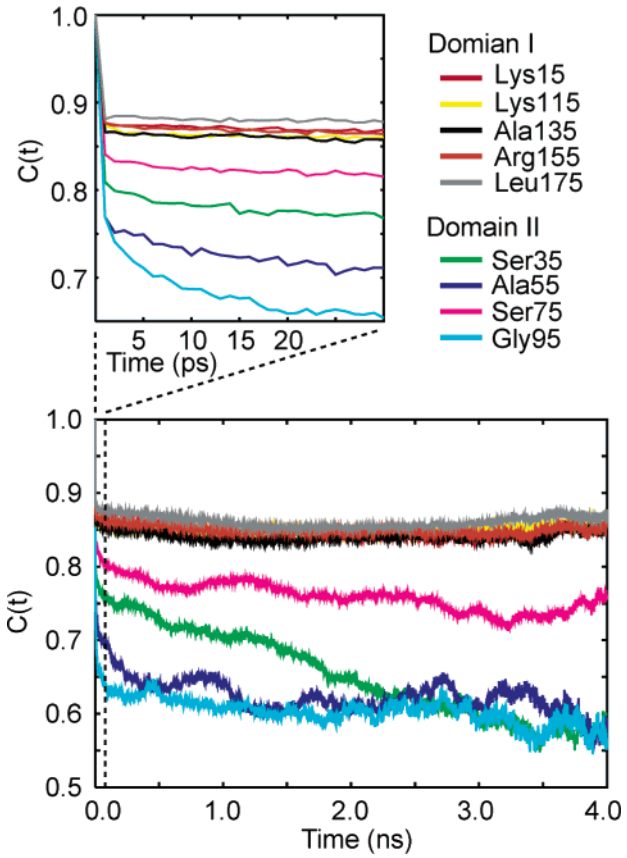

FIGURE 4: Correlation functions for internal motion of NH vectors of several residues calculated from 1.5 ns MD trajectory.

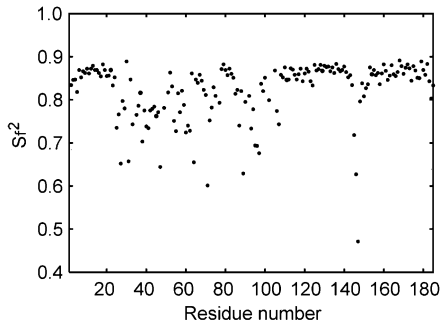

FIGURE 5: Order parameters for fast internal motion calculated from MD trajectories of *E. coli* RRF. Values were obtained from the correlation functions at 15 ps.

for domain II is significantly larger (0.5 Å on average) than that for domain I (0.1 Å) and vice versa. Interestingly, the time evolutions of RMSD show an oscillation from 0.2 to 1.0 Å on a nanosecond time scale.

Figure 4 shows typical profiles of correlation functions for internal motion of N−H vectors obtained from MD trajectory. An initial drop during the first a few picoseconds is observed for all residues. After this burst phase, most of the correlation functions of residues in domain I decrease very slowly. However, correlation functions of many residues in domain II show more complex behavior. Several residues indicate oscillation of correlation functions. The order parameters for fast local motion, S_f^2, which were estimated from eq 3, are presented in Figure 5. S_f^2 has a quite uniform value of about 0.87 in the α helix region. In the β sheet region, S_f^2 values are distributed in a range between 0.75 and 0.85. In the peptide segments between

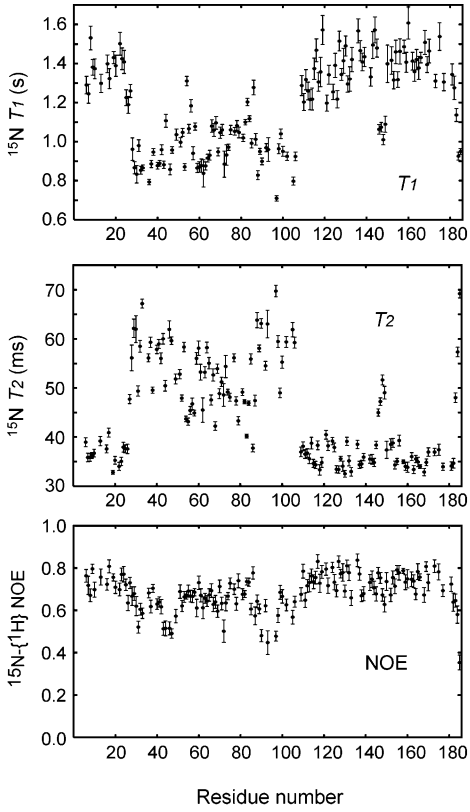

FIGURE 6: ^{15}N relaxation data at 30 °C and at 1H frequency of 600 MHz for *E. coli* RRF. Error bars indicate standard deviations of data obtained by least squares.

Table 1: Results of Simple Model-Free Analysis for ^{15}N Relaxation Data of RRF

domain	$\tau_{c,eff}$ (ns)	A	S^2	τ (ps)	MSE[a]
I	18.6	1.47	0.94	142	9.0
II	13.8	1.89	0.90	444	14.7
all	14.8	2.40	0.92	168	16.4

[a] Mean squared error defined by χ^2 divided by the degree of freedom of fitting.

regular secondary structures, most of S_f^2 values are lower than 0.7.

NMR Relaxation Measurements. Almost all resonances expected to give peaks in ^{1}H-^{15}N HSQC spectra were observed. However, very weak or overlapping resonances are difficult to quantify for spin relaxation measurements. Among 185 residues, T_1, T_2, and ^{15}N-{^{1}H} NOE values from 140 residues for *E. coli* RRF were obtained. The relaxation measurements were repeated twice, and the pairwise rms differences were 5% for T_1, 3% for T_2, and 5% for NOE. The analyzed T_1, T_2, and ^{15}N-{^{1}H} NOE values are presented in Figure 6. The distribution of these values clearly shows a bimodal profile, which is similar to that observed in the case of *A. aeolicus* RRF (*8*). Such profiles indicate that *E. coli* RRF has a characteristic two domain structure in solution.

Relaxation Analysis. The results of simple model-free analyses are shown in Table 1. The large values of the mean squared errors for whole molecule show that the quality of fit in simple model-free approach is poor. The averaged values of calculated order parameters are significantly larger than the normal value obtained in the well-defined region of protein, which is generally about 0.85. Furthermore, the experimental correlation times for local motion, τ, are slightly larger than the expected value for fast vibrational motion. Such results suggest that some motion exists that has not been considered in the simple model-free approach.

Table 2: Results of Extended Model-Free Analysis for ^{15}N Relaxation Data of RRF

domain	$\tau_{c,eff}$ (ns)	A	S_s^2	τ_s (ns)	MSE[a]
I			0.89	2.1	
II			0.73	1.9	
all	21.8	1.81			7.4

[a] Mean squared error defined by χ^2 divided by the degree of freedom of fitting.

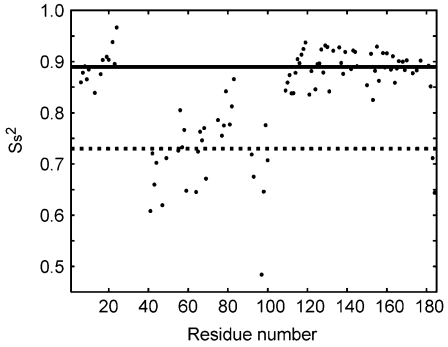

FIGURE 7: Order parameters for slow domain motion (S_s^2) obtained from extended model-free calculation. Solid line and dashed line represent 0.89 and 0.73, which are the mean values of S_s^2 for domains I and II, respectively. The outliers, Asp97, Met183, and Gln184, are excluded for calculation of the mean values.

The effective correlation times for domains I and II are 18.6 and 13.8 ns, respectively. The ratio between these values is 1.35. The deviation from unity suggests that these domains do not tumble as a rigid entity and that nanosecond ordered domain motions are present. Therefore, we applied the extended spectral density function to account for such motion. The results of such analyses are shown in Table 2 and Figure 7. It is noteworthy that the value of the mean squared errors substantially decrease in this model as compared with that in simple model-free analyses. A small residual indicates the extended model is more meaningful. The overall correlation time is 21.8 ns while internal motions of domains on a time scale of 2 ns were obtained. The optimized order parameters (S_s^2) in domains I and II of *E. coli* RRF are distributed in the ranges of 0.89 ± 0.03 and 0.73 ± 0.07, respectively.

DISCUSSION

Although the importance of ribosome recycling step for cell viability and an essential role of RRF in that step have been reported earlier, the detailed mechanism of the ribosome recycling process by RRF has not been established. Recently, the importance of the fluctuation in interdomain orientation was suggested from some genetic experiments (*6, 12*). In this study, a characterization and a quantification of internal motion of the RRF molecule are presented.

The structure of RRF is structurally divided into two domains. As shown in Figure 3, the RMSD value for each domain is about 0.1 Å during MD simulation. This result

supports the likelihood that each structural domain of RRF behaves as a rigid body. On the other hand, the spatial arrangement of the domains varies on a nanosecond time scale. The essential dynamics analysis shows that each domain undergoes a dominant collective motion. As shown in Figure 2, this motion can be described as a limited rotation of domain II, approximately 11°, around the bundle axis of domain I. In that motion, the characteristic L-shape structure of RRF as a mimic of tRNA is maintained. This nature of dynamics in the RRF molecule had been suggested by a comparison of crystal structures (*6*) with the NMR determined structure ensemble (*8*). Because the length of MD simulation was limited to 4.5 ns, the rare events that change domain orientation significantly may not have been sampled. Thus, the range of domain motion in MD simulation corresponds to the lower limit.

The simple model-free analysis of ^{15}N relaxation data, where domain fluctuation was not considered, gave poor quality of fit. In that analysis, the calculated order parameters may be overestimated. That anomaly could be explained as follows. In the procedure of the simple model-free analysis, the T_1/T_2 ratio, which is not influenced by fast internal motion, is used to estimate overall correlation time (τ_c). However, T_1/T_2 is actually reduced when a significant slow global motion exists. In such a case, τ_c is underestimated. The order parameter calculated by the simple model-free analysis corresponds to the ratio of the experimentally obtained spectral density to the estimated τ_c at zero frequency. As a result, the order parameter is overestimated when a slow global motion exists. In general, such an effect should be considered when dynamics of a multidomain protein is analyzed by the simple model-free approach.

The ratio of τ_cs between domains I and II, 1.35, indicates that domain I is more restricted spatially than domain II, although it is difficult to quantify the mobility in relative orientation of domains by the simple model-free analysis. Then, we attempted to interpret experimental data using an extended model-free spectral density function. Although similar applications of that function for analyzing slow interdomain motion of Ca^{2+}-ligated calmodulin and FBP3/4-M29 complex using multiple field experiments were recently reported (*33*, *34*), our approach is somewhat different from theirs. We employed an approach where MD simulation was used to complement NMR experiments at a single field. As mentioned in the literature, the analysis of relaxation data measured at multiple fields is very useful to detect such a slow global motion in multidomain protein and is superior in the point that it requires experimental data only without any a priori assumptions for parameters. However, NMR experiments at multiple fields also present some difficulties. At high field, the contribution of chemical exchange and variations in chemical shift anisotropy are increased. At low field, resolution and sensitivity become problems for large proteins. Indeed, when we tried to obtain a set of NMR data at 500 MHz of ^1H frequency, a severe spectral overlapping made a quantitative analysis difficult. From the analysis of MD trajectory, order parameters for local fast motion (S_f^2) can be derived (*36*). Thus, from relaxation data at a single field, we could reduce the number of variables so as to determine parameters for both rotational diffusion of the molecule and domain motion. Of course, our method and reported ones are not exclusive. The combination and comparison of both approaches might provide further insights into domain motion of proteins and are in progress. Furthermore, instead of optimizing the order parameter for the motion on a slow time scale, S_s, per domain, we optimized that value per residue. The structures of two domains of RRF are not similar to each other, and the relative rotation of domains is allowed within a limited direction. These are properties different from those of dumbbell-like molecules in which the applications of extended model-free analysis have been reported (*33*, *34*). In the case of RRF, each residue would not experience a unique motion even in a domain. Therefore, we assigned a S_s value per residue.

The mean value of order parameter for slow domain motion (S_s^2) in domain I of *E. coli* RRF was 0.89 ± 0.03. This value indicates that domain I of the RRF molecule is nearly fixed on the diffusion frame of the molecule. On the other hand, the mean value of S_s^2 in domain II was 0.73 ± 0.07 and indicates that domain II of RRF is more flexible than domain I. Considering that each domain would diffuse in a cone of semi-angle θ, the observed order parameters correspond to a θ of 16° for domain I and to a θ of 26° for domain II. Interestingly, in domain II, S_s^2 values of the α helix are relatively larger (0.80 ± 0.04) than those of the β sheet region (0.71 ± 0.05). There are two possible reasons for the variety of S_s^2 values within the same domain. One is that the internal motion in domain II occurs on a medium time scale. When such motion exists, the domain motion may be overestimated. Another possibility is that the variations in calculated S_s^2 values in a domain indicate that the motion of each domain is anisotropic, not isotropic free diffusion. Such anisotropic domain motion has been indicated in the analysis of MD simulation. Modulation of spectral density function by anisotropic motion is dependent on the averaged orientation of the internuclear vector. Therefore, the analyses of the correlation between S_s^2 values and the orientation of the internuclear vector should provide information about the anisotropy of domain motion (e.g., the axis of rotation). Actually, we could not detect such correlations. Because the N−H internuclear vectors distribute within a narrow range in a three helix bundle of domain I and in β sheets of domain II, the directional information may be insufficient to obtain such correlations. The analyses on relaxation of other nuclei that sample a different direction (e.g., $^{13}C\alpha$ and $^{13}C'$) may help for solving this problem and are in progress.

The goal of this work is to clarify the contribution of internal motion and/or plasticity of RRF to the ribosome recycling process. We have demonstrated that the combination of MD calculation and NMR relaxation analysis is a powerful strategy for analyzing intramolecular dynamics of RRF. In this study, the MD simulation has revealed that each domain of the RRF molecule undergoes a collective motion. The variation of relative arrangement between domains is described as a limited rotation around a hinge axis, which is nearly parallel to the bundle axis of domain I. The tRNA mimicking L-shape of RRF was shown to be maintained during such rotation. This NMR study demonstrates that the range of rotation of domain II in solution is about 30° as a cone semi-angle. These results indicate that the joint regions between the domains are flexible and relative arrangement of the domains can be easily changed in a certain direction

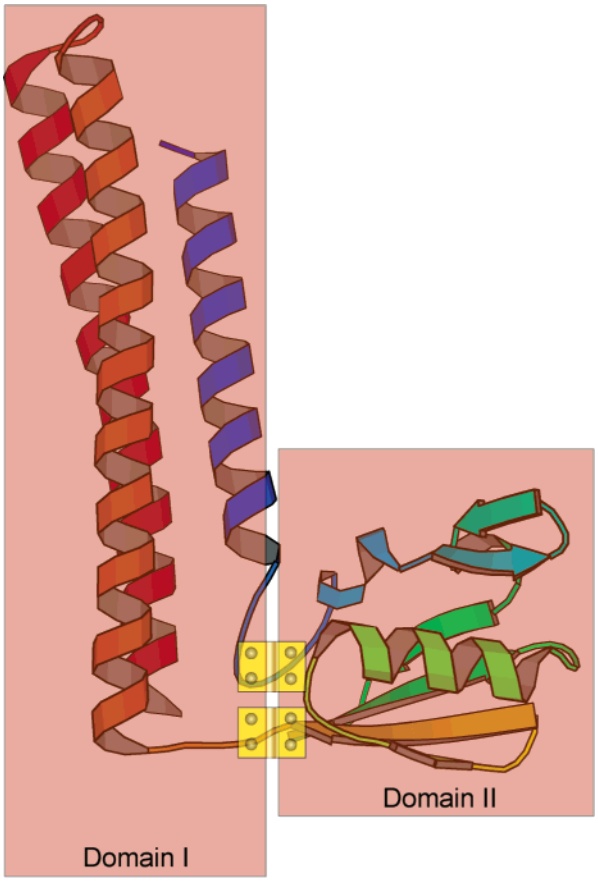

FIGURE 8: Spatial arrangement of two peptide chains of the joint region between domains I and II as modeled by a swinging door.

by an external force. The characteristic dynamics of the RRF molecule may be attributed to the geometry of peptide chains in joint regions, which is presented in Figure 8. Because the two peptide chains of joint regions are arranged nearly vertically about the bundle axis of domain I like two hinges of a door, the bending angle between domains is maintained at a right angle. But domain II is able to flap by swinging around the bundle axis of domain I. As the amino acid sequence of joint regions are well-conserved in RRFs (*6*), the characteristic dynamics of the RRF molecule is likely to be conserved evolutionally to contribute to its activity. Recently, we proposed a model for the binding mode of RRF to ribosome where domain I is bound to the 50S subunit and domain II does not participate in ribosome binding at the A-site (*7*). In that model, domain II is able to change its position toward the P-site as mentioned above. The conformational change of EF-G upon GTP hydrolysis could be transmitted through this movement of domain II to the P-site bound tRNA; consequently, RRF may help release tRNA thereby resulting in ribosome recycling reaction.

REFERENCES

1. Janosi, L., Hara, H., Zhang, S., and Kaji, A. (1996) *Adv. Biophys. 32*, 121−201.
2. Kaji, A., and Hirokawa, G. (2000) Ribosome-Recycling Factor: an Essential Factor for Protein Synthesis, in *The Ribosome*: *Structure, Function, Antibiotics and Cellular Interactions* (Garret, R. A., Douthwaite, S. R., Liljas, A., Matheson, A. T., Moore, P. B., and Noller, H. F., Eds.) pp 527−539, ASM Press, Washington, DC.
3. Selmer, M., Al-Karadaghi, S., Hirokawa, G., Kaji, A., and Liljas, A. (1999) *Science 286*, 2349−2352.
4. Kim, K. K., Min, K., and Suh, S. W. (2000) *EMBO J. 19*, 2362−2370.
5. Nakano, H., Uchiyama, S., Yoshida, T., Ohkubo, T., Kato, H., Yamagata, Y., and Kobayashi, Y. (2002) *Acta Crystallogr. D58*, 124−126.
6. Toyoda, T., Tin, O. F., Ito, K., Fujiwara, T., Kumasaka, T., Yamamoto, M., Garber, M. B., and Nakamura, Y. (2000) *RNA 6*, 1432−1444.
7. Nakano, H., Yoshida, T., Uchiyama, S., Kawachi, M., Matuo, H., Kato, T., Ohshima, A., Yamaichi, Y., Honda, T., Kato, H., Yamagata, Y., Ohkubo, T., and Kobayashi, Y. (2003) *J. Biol. Chem. 278*, 3427−3436.
8. Yoshida, T., Uchiyama, S., Nakano, H., Kashimori, H., Kijima, H., Ohsima, T., Saihara, Y., Ishino, T., Shimahara, H., Yoshida, T., Yokose, K., Ohkubo, T., Kaji, A., and Kobayashi, Y. (2001) *Biochemistry 40*, 2387−2396.
9. Hirokawa G., Kiel, M. C., Muto A., Selmer, M., Raj, V. S., Lilijas, A., Igarashi, K., Kaji, H., and Kaji, A. (2002) *EMBO J. 21*, 2272−2281.
10. Rao, A. R., and Varshney, U. (2001) *EMBO J. 20*, 2977−2986.
11. Ito, K., Fujiwara, T., Toyoda, T., and Nakamura, Y. (2002) *Mol. Cell 9*, 1263−1272
12. Atarashi, K., and Kaji, A. (2000) *J. Bacteriol. 182*, 6154−6160.
13. Berendsen, H. J. C., van der Spoel, D., and van Drunen, R. (1995) *Comput. Phys. Comm. 91*, 43−65.
14. Lindahl, E., Hess, B., and van der Spoel, D. (2001) *J. Mol. Mod. 7*, 306−317.
15. Berendsen, H. J. C., Postma, J. P. M., van Gunsteren, W. F., and Harmans, J. (1981) in *Intermolecular Forces* (Pullman, B., Ed.) pp 331−342, Reidel, Dordrecht.
16. Darden, T., York, D., and Pedersen, L. (1993) *J. Chem. Phys. 98*, 10089−10092.
17. Hess, B., Bekker, H., Berendsen, H. L. C., and Fraaije, J. G. E. M. (1997) *J. Comput. Chem. 18*, 1463−1472.
18. Berendsen, H. J. C., Postma, J. P. M., DiNola, A., and Haak, J. R. (1984) *J. Chem. Phys. 81*, 3684−3690.
19. Amadei, A., Linssen, A. B. M., Berendsen, H. J. C. (1993) *Proteins*: *Struct. Funct. Gen. 17*, 412−425.
20. Lipari, G., and Szabo, A. (1982) *J. Am. Chem. Soc. 104*, 4546−4559.
21. Lipari, G., and Szabo, A. (1982) *J. Am. Chem. Soc. 104*, 4559−4570.
22. Peng, J. W., Thanabal, V., and Wagner, G. (1991) *J. Magn. Reson. 95*, 421−427.
23. Kay, L. E, Nicholson, L. K., Delaglio, F., Bax, A., and Torchia, D. (1992) *J. Magn. Reson. 97*, 359−375.
24. Grzesiek, S., and Bax, A. (1993) *J. Am. Chem. Soc. 115*, 12593−12594.
25. Delaglio, F., Grzesiek, S., Vuister, G. W., Zhu, G., Pfeifer, J., and Bax, A. (1995) *J. Biomol. NMR 6*, 277−293.
26. Garrett, D. S., Powers, R., Gronenborn, A. M., and Clore, G. M. (1991) *J. Magn. Reson. 95*, 214−220.
27. Yoshida, T., Kijima, H., Oka, S., Uchiyama, S., Nakano, H., Ohkubo, T., and Kobayashi, Y. (2002) *J. Biomol. NMR 22*, 195−196
28. Tjandra, N., Wingfield, P., Stahl, S., Bax, A. (1996) *J. Biomol. NMR 8*, 273−284.
29. Abragam, A. (1961) *The principles of Nuclear Magnetic Resonance*, Clarendon Press, Oxford.
30. Kroenke, C. D., Rance, M., and Palmer, A. G. (1999) *J. Am. Chem. Soc. 121*, 10119−10125
31. Mandel, A. M., Akke, M., and Palmer, A. G. (1995) *J. Mol. Biol. 246*, 144−163.
32. Clore, G. M., Szabo, A., Bax, A., Kay, L. E., Driscoll, P. C., and Gronenborn, A. M. (1990) *J. Am. Chem. Soc. 112*, 4989−4991.
33. Baber, J. L., Szabo, A., and Tjandra, N. (2001) *J. Am. Chem. Soc. 123*, 3953−3959.
34. Braddock, D. T., Louis, J. M., Baber, J. L., Levens, D., and Clore, G. M. (2002) *Nature 415*, 1051−1056.
35. Komeji, Y., Uebayashi, M., and Yamato, I. (1994) *Proteins 20*, 248−258.
36. Philippopoulos, M., Mandel, A. M., Palmer, A. G., and Lim, C. (1997) *Proteins 28*, 481−493.

BI027191Y